Robust Barcode Decoding from Degraded Images Using YOLOv11 and Signal-based Reconstruction

Panupong Chaiyarat [1] and Chaiyong Soemphol [2,*]
[1] Department of Electrical and Computer Engineering, Faculty of Eng., Mahasarakham University, Mahasarakham, Thailand
[2] Research Unit for Electrical and Computer Engineering Technology, Faculty of Engineering, Mahasarakham University, Maha Sarakham, Thailand
Email: 68010383501@msu.ac.th (P.C.); chaiyong.s@msu.ac.th (C.S.)

Manuscript received June 17, 2026; revised July 9, 2026; accepted September 1, 2026; published November 25, 2026
*Corresponding author

***Abstract*—Reliable barcode decoding from camera-captured images remains challenging in industrial environments due to blur, reflections, uneven illumination, and label degradation. This paper proposes an automated barcode decoding framework, specifically tailored for Interleaved Two of Five (ITF) symbology, that integrates YOLOv11s localization with a four-stage decoding pipeline comprising direct decoding, image enhancement, multi-library decoding, and a novel signal-based reconstruction method. The proposed reconstruction stage converts barcode regions into one-dimensional vertical projection profiles, performs adaptive signal repair, and reconstructs synthetic barcode images for final decoding. The framework was evaluated on 12,050 Interleaved Two of Five (ITF) barcodes extracted from 500 real-world airline baggage-tag images exhibiting significant visual degradation. Experimental results show that the YOLOv11s detector achieved 99.61% precision and 99.3% mAP@0.5, ensuring reliable barcode localization. The proposed framework achieved an exact decoding accuracy of 96.01%, correctly decoding 11,569 out of 12,050 barcode instances. Decoding pipeline analysis confirmed that the progressive decoding architecture effectively balances accuracy and computational cost, while the signal-based reconstruction stage successfully recovered severely degraded barcodes that could not be decoded using conventional image-domain techniques. These findings demonstrate that combining deep-learning-based localization with signal-domain structural recovery offers a robust and practical solution for barcode decoding in real-world industrial applications.**

***Index Terms*—barcode decoding, YOLOv11s, signal-based reconstruction, computer vision, industrial logistics**

I. Introduction

One-Dimensional (1D) barcodes, such as EAN-13, Code 128, and Interleaved Two of Five (ITF), remain essential in logistics and industrial operations because they provide reliable machine-readable identification for products and logistics units, supporting inventory management, traceability, and operational efficiency across supply chains [1, 2]. In applications including warehousing, manufacturing, and airport baggage handling, decoding accuracy directly influences operational efficiency, traceability, and safety [3]. Although laser scanners provide highly reliable decoding under controlled conditions, many modern systems increasingly rely on camera-based acquisition because of their lower cost, greater flexibility, and seamless integration with computer vision technologies. Recent advances in computer vision and deep learning have further expanded barcode-related research, encompassing detection, localization, classification, and decoding tasks [4].

However, barcode images captured by cameras are often affected by motion blur, uneven illumination, reflections, perspective distortion, and label deterioration such as fading, abrasion, or tearing [5, 6]. These degradations reduce the structural integrity of barcode patterns and adversely affect the distinct bar-space transitions required for reliable decoding. Consequently, conventional barcode decoders, including ZXing-based and ZBar-based implementations, often experience reduced decoding accuracy under low-contrast, blurred, or noisy imaging conditions [7].

Previous studies have approached barcode analysis through three main directions: localization, image enhancement, and signal-based decoding. Deep-learning detectors, particularly the YOLO family [8–10], have demonstrated robust barcode localization in unconstrained environments. Studies by Hansen *et al*. [11] and Xiao and Ming [12] reported superior detection accuracy and speed compared with traditional geometric approaches, while feature pyramid networks improve multi-scale representation and small-object detection [13]. Nevertheless, these methods primarily focus on localization rather than reliable decoding of degraded barcode regions.

Image restoration techniques, including neural deblurring, super-resolution, and morphological enhancement methods, have been widely investigated for improving barcode readability under adverse imaging conditions [14–17]. Although these approaches can enhance visual quality and recover fine structural details, their effectiveness often depends on degradation-specific

doi: 10.18178/ijeetc.15.6.438-447

assumptions and training data, limiting generalization across diverse real-world environments. Furthermore, improved visual appearance does not necessarily guarantee successful barcode decoding, as reconstruction artifacts may still disrupt critical bar-space transitions [18]. Alternatively, signal-domain approaches have shown that barcode structures can remain recoverable even when image quality is severely compromised [19–21]. However, such methods have rarely been integrated with modern deep-learning-based localization frameworks or evaluated within a complete end-to-end decoding system.

As a result, a significant gap persists between accurate barcode detection and dependable decoding in challenging real-world conditions. Existing solutions typically treat localization and restoration as separate tasks, while the potential of exploiting barcode periodicity and deterministic bar–space patterns for structural recovery remains underexplored.

To address this limitation, this study presents an automated barcode decoding framework that combines YOLOv11s detection with a multi-stage decoding pipeline. The framework applies progressively more advanced decoding strategies, enabling efficient processing of readable barcodes while reserving computationally intensive recovery procedures for severely degraded samples.

Furthermore, since this study focuses on barcode recognition in airline baggage-handling systems, the proposed framework is specifically optimized for Interleaved Two of Five (ITF) barcodes. Unlike conventional one-dimensional signal scanning approaches, such as single-scanline methods that sample a limited line of pixels and may fail when the selected line is severely degraded, the proposed Vertical Projection Profile (VPP) approach aggregates information across the entire localized two-dimensional barcode Region of Interest (ROI) and transforms it into a one-dimensional signal representation before decoding. This enables information from multiple image columns to contribute to the reconstructed barcode signal, reducing the dependence on any single potentially degraded scanline.

II. Proposed Framework and Experimental Setup

This section presents the proposed framework for robust barcode decoding from degraded images. The framework integrates YOLOv11s-based localization with a progressive multi-stage decoding pipeline that applies increasingly sophisticated recovery strategies only when required. Particular emphasis is placed on the proposed signal-based reconstruction algorithm, which reformulates barcode recovery as a one-dimensional signal restoration problem. The following subsections describe the system architecture, detector design, decoding stages, and evaluation dataset in detail.

A. System Overview and Dataset

The proposed framework aims to achieve reliable barcode decoding under severe real-world image degradation while maintaining computational efficiency. As shown in Fig. 1, the system comprises three main components: 1) barcode localization using YOLOv11s, 2) a four-stage progressive decoding pipeline with early-exit functionality, and 3) a signal-based reconstruction module for recovering severely degraded barcodes.

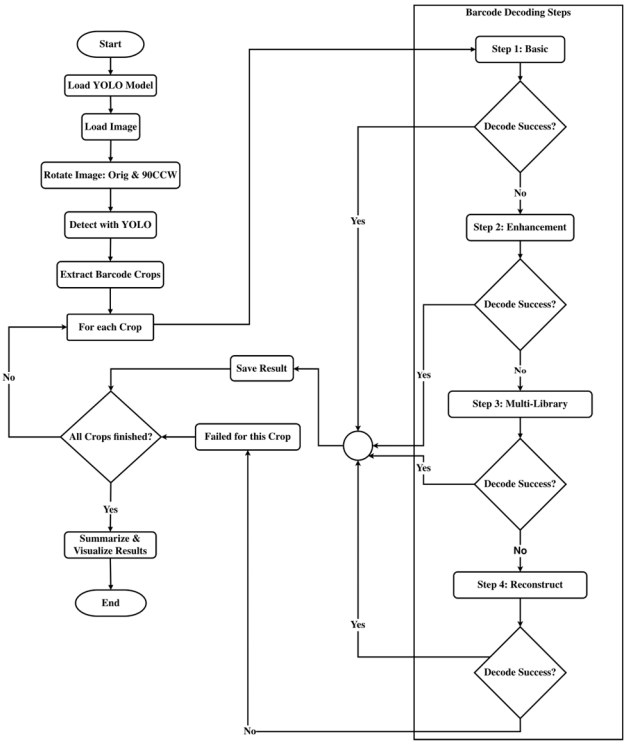

Fig. 1. Overall framework architecture.

The processing workflow begins with barcode localization. Given an input image, YOLOv11s detects barcode regions and extracts the corresponding Regions of Interest (ROI). Each ROI is then passed through the decoding pipeline, which is arranged from low-cost operations to increasingly sophisticated recovery strategies. Successful decoding at any stage immediately terminates further processing for that ROI, minimizing unnecessary computation. Only unresolved cases proceed to the final signal-based reconstruction stage.

The framework was developed in Python using OpenCV [22], Ultralytics YOLO [23], Pyzbar, ZXing-cpp, and NumPy. Model training was conducted on Google Colab with a Tesla T4 GPU (14,913 MiB VRAM), whereas all decoding experiments were performed on CPU hardware to assess deployment feasibility without specialised acceleration.

Evaluation was conducted on a dataset of 500 real-world images containing 12,050 ITF barcodes collected from an airline baggage reconciliation system. The dataset includes diverse degradation factors, such as motion blur, uneven illumination, specular reflections, partial occlusion, faded printing, and physical label damage. Representative examples are shown in Fig. 2.

Although the dataset contains 12,050 barcode instances extracted from 500 original images, individual barcode labels were printed and handled independently before being attached to the tracking sheets. Consequently, the

instances exhibit diverse barcode-level degradation characteristics, including physical creases, tears, skewed orientations, ink fading, and smudging caused by handling. However, barcode instances originating from the same image may share common environmental characteristics, such as background and illumination. Therefore, the 12,050 instances provide substantial barcode-level variation, while the number of unique image frames remains a limitation in terms of environmental diversity. Future work will evaluate the proposed framework using larger datasets with greater variation in backgrounds, illumination, viewpoints, and acquisition conditions.

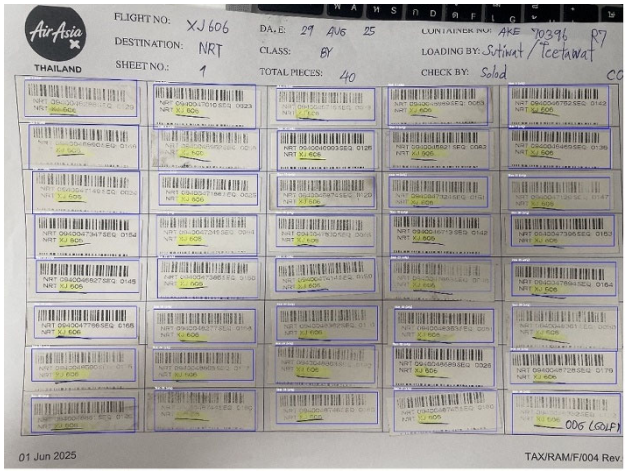

Fig. 2. Samples from the airline baggage-tag dataset.

The complete collected dataset consists of 1000 real-world images, which were partitioned into two independent groups of 500 images each. The first group was used for barcode localization network development and YOLOv11s detector training. A frame-level split was applied, with 400 images allocated for training and 100 independent images reserved for validation. This strategy ensured that barcode instances originating from the same image frame did not appear in both the training and validation sets. The second group of 500 images remained completely unseen during both detector training and validation and was used exclusively for the final evaluation of the downstream multi-stage decoding pipeline. From these images, 12,050 cropped barcode instances were extracted and processed to assess decoding robustness under severe real-world visual degradations. This separation ensures that the final decoding evaluation was conducted using image frames independent of those used for detector development. Ground-truth barcode values were established from the Human-Readable Interpretation (HRI) printed on each baggage tag and were carefully cross-checked to ensure annotation accuracy.

B. YOLOv11s Barcode Detector

Barcode localization was performed using YOLOv11s. The model was fine-tuned for 15 epochs using the AdamW optimizer [24] with a learning rate of 0.002 and momentum of 0.9. All training images were resized to 1280 × 1280 pixels to improve the detection of small and partially degraded barcode instances.

To improve robustness to orientation variations, each image is evaluated twice during inference: once in its original orientation and once after a 90° counterclockwise rotation. Detections from both passes are then combined prior to ROI extraction. This dual-orientation approach increases the detection reliability of vertically aligned baggage-tag barcodes without requiring additional model training. The resulting bounding boxes define the barcode ROIs, which are subsequently forwarded to the decoding pipeline described in the following subsection.

C. Multi-stage Decoding Pipeline

The proposed decoding framework adopts a progressive multi-stage architecture that balances decoding accuracy with computational efficiency. Rather than applying expensive restoration techniques to every barcode region, decoding is performed incrementally using increasingly advanced processing strategies. This early-exit design enables rapid decoding of readable barcodes while reserving intensive recovery procedures for severely degraded samples. Each ROI passes sequentially through four stages, and processing stops immediately once a valid barcode is obtained.

The first stage attempts direct decoding of the raw ROI using Pyzbar without any preprocessing. This provides a low-cost decoding pathway for high-quality barcode images and avoids unnecessary processing when barcode structures remain sufficiently intact.

ROIs that cannot be decoded in the first stage undergo image enhancement to improve bar-space contrast and reduce image noise. The enhancement pipeline includes grayscale conversion, bilateral filtering, CLAHE-based contrast enhancement [25], and gamma correction. Grayscale conversion removes color redundancy, while bilateral filtering suppresses noise without compromising edge information [26]. CLAHE improves local contrast under uneven illumination, and gamma correction enhances visibility in darker image regions. The enhanced image is then binarized using Otsu thresholding [27], followed by a second decoding attempt with Pyzbar.

Barcodes unresolved after image enhancement may still contain recoverable structural information under alternative preprocessing conditions. Therefore, the third stage performs a comprehensive search across multiple preprocessing configurations and decoding libraries. The evaluated preprocessing operations include Otsu thresholding, adaptive thresholding, morphological closing, image scaling, dilation, and erosion. Each generated image variant is decoded using both Pyzbar and ZXing-cpp. By combining diverse preprocessing strategies with complementary decoding libraries, this stage improves robustness to blur, contrast degradation, and structural discontinuities.

To ensure a fair comparison, the same localized barcode ROIs generated by the YOLOv11s detector were provided as input to the proposed framework, ZXing, and Pyzbar. Therefore, all methods were evaluated using identical barcode patches, allowing the comparison to focus on their decoding capabilities under the same localization

conditions. The standalone baseline libraries were not applied to raw, unlocalized full images.

Barcodes that remain unresolved after the preceding stages are forwarded to the proposed signal-based reconstruction module. Unlike conventional image-domain approaches, this stage recovers barcode information in the one-dimensional signal domain by exploiting the periodic structure of barcode patterns. The method converts barcode regions into vertical projection profiles, performs adaptive signal repair, and reconstructs synthetic barcode images for final decoding. A detailed description of the reconstruction algorithm is provided in Section D.

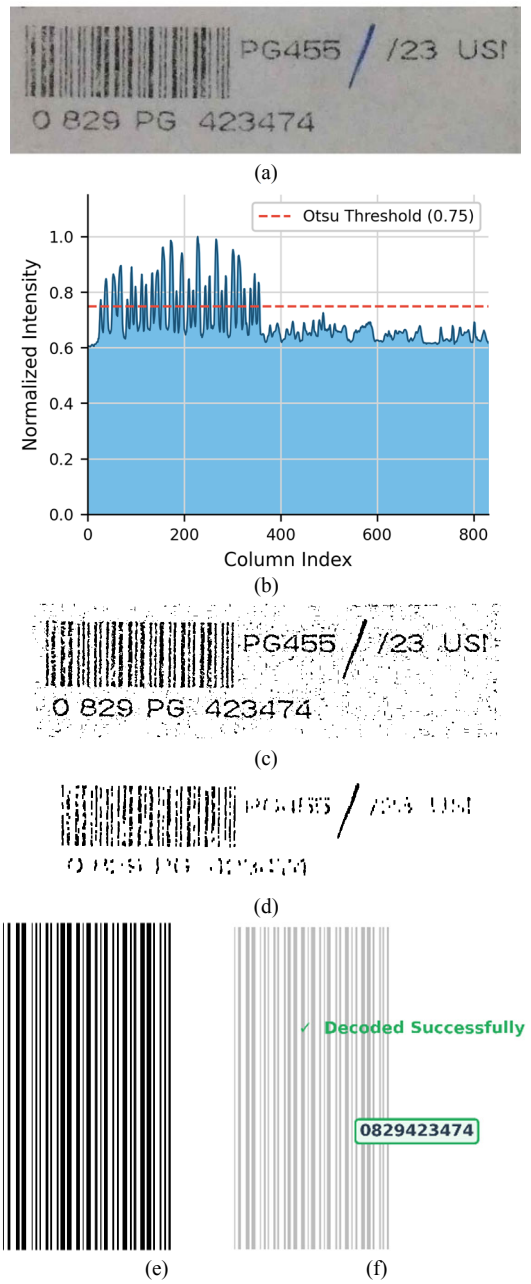

Fig. 3. Signal-based reconstruction process: (a) Original barcode ROI, (b) vertical projection profile, (c) adaptive thresholding, (d) morphological signal repair, (e) synthetic barcode reconstruction, and (f) successful decoding.

D. Signal-based Reconstruction

Signal-based reconstruction is the principal methodological contribution of this study. Unlike conventional image-domain approaches that rely on preserving pixel-level barcode structures, the proposed method reformulates barcode recovery as a one-dimensional signal restoration problem. By exploiting the periodic bar-space characteristics of barcode patterns, the method can recover structural information that remains difficult to reconstruct using conventional image enhancement techniques. The overall reconstruction process is illustrated in Fig. 3.

1) Image-to-signal conversion

Given a grayscale barcode ROI, the image is optionally upscaled and converted into a one-dimensional Vertical Projection Profile (VPP) by averaging pixel intensities $P(x)$ along each image column as in Eq. (1):

$$P(x) = \frac{1}{H}\sum_{y=0}^{H-1} I(x,y) \quad (1)$$

where $I(x, y)$ denotes the grayscale intensity at pixel (x, y), and H represents the image height.

This transformation effectively acts as a spatial low-pass filter, reducing local image noise while preserving the periodic bar-space structure characteristic of one-dimensional barcodes.

2) Adaptive signal thresholding

Barcode images often exhibit non-uniform illumination, making fixed global thresholds unreliable. To address this issue, the projection signal is converted into a binary signal, $B(x)$, using an adaptive moving-average thresholding scheme, as expressed in Eq. (2):

$$B(x) = \begin{cases} 1, & P(x) < \mu_w(x) - \delta \\ 0, & \text{otherwise} \end{cases} \quad (2)$$

where $B(x)$ denotes the binarized projection signal at position x, $\mu_w(x)$ is the local moving average computed within a window of size w (set to 50 pixels), and δ is an adaptive offset parameter (set to 15) with a minimum signal strength threshold of 50.

By adapting to local intensity variations, this approach improves robustness to shadows, reflections, and uneven lighting.

3) Morphological signal repair

Following binarization, the signal may still contain fragmented barcode structures caused by blur, occlusion, or physical label damage. To restore structural continuity, three sequential one-dimensional morphological operations are applied: 1) thin-bar expansion to strengthen weak barcode segments, 2) gap closing to bridge short interruptions within barcode bars, and 3) fragment merging to reconnect adjacent disconnected structures.

Performing these operations directly in the signal domain preserves barcode periodicity while significantly reducing computational complexity compared with conventional image-based morphology.

4) Synthetic barcode reconstruction

The repaired binary signal is vertically replicated to generate a high-contrast synthetic barcode image consisting of black bars on a white background. This process removes residual background artefacts and restores the clear bar-space transitions required for reliable decoding.

To improve robustness across varying degradation conditions, multiple thresholding and signal-repair parameter combinations are evaluated during reconstruction. The reconstruction process utilizes an input upscale factor of 2.0 or 3.0, a minimum bar width constraint of 7 pixels, a global minimum intensity threshold of 20, and a maximum gap fill size of 3 pixels. Processing terminates immediately once a valid barcode satisfying the expected structural constraints is successfully decoded.

III. Results and Discussion

This section presents the experimental evaluation of the proposed framework. First, the performance of the YOLOv11s detector is assessed in terms of barcode localization accuracy. Subsequently, the effectiveness of the proposed decoding pipeline and signal-based reconstruction method is analyzed through comparative and stage-wise experiments.

A. YOLOv11s Detection Performance

The YOLOv11s detector was evaluated on a validation set comprising 100 images containing 2571 annotated barcode instances. The model was fine-tuned using an early stopping mechanism with a patience of 5 epochs. Training converged within 15 epochs without evidence of overfitting. Both the training and validation losses decreased consistently without divergence, while the training and validation performance remained closely aligned throughout the training process, as shown in Fig. 4. These observations indicate stable convergence and good generalization to the validation set.

The quantitative performance of the YOLOv11s detector is summarized in Table I. The detector achieved a precision of 99.61%, recall of 99.96%, mAP@0.5 of 99.3%, and mAP@0.5:0.95 of 97.5%. The confusion matrix reported 2570 true positives, ten false positives, and one false negative, indicating highly accurate localization with minimal detection errors. In addition, the Precision-Recall curve exhibited an Area under the Curve (AUC) of 0.993, demonstrating consistently strong performance across a wide range of confidence thresholds.

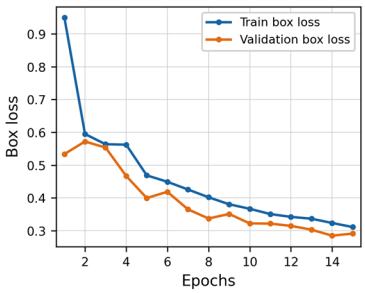

(a)

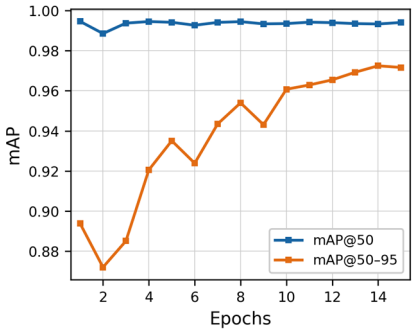

(b)

Fig. 4. Training performance of the YOLOv11s detector over 15 epochs: (a) training and validation bounding-box loss and (b) mAP@50 and mAP@50–95.

These results confirm that YOLOv11s provides reliable barcode localization under challenging imaging conditions, including perspective distortion, uneven illumination, and partial barcode degradation. Accurate ROI extraction is essential for downstream decoding, as incomplete crops or imprecise boundaries can adversely affect decoding success. The proposed dual-orientation inference strategy further enhances detection robustness for vertically aligned baggage-tag barcodes commonly encountered in airline baggage reconciliation systems.

TABLE I: Detection Performance of the YOLOv11s Barcode Localization Model

Detection Metric	Value
Precision	99.61%
Recall	99.96%
mAP@0.5	99.30%
mAP@0.5:0.95	97.50%
AUC (Precision–Recall)	0.993
True Positives	2570
False Positives	10
False Negatives	1
Inference Time	39.1 ms/image

B. Comparative Decoding Performance

The proposed framework was evaluated on a dataset of 12,050 ITF barcodes extracted from 500 real-world airline baggage-tag images. Table II presents a performance comparison with two widely used barcode decoding libraries, Pyzbar and ZXing. To ensure a fair and symmetric comparison, the standalone baseline libraries (Pyzbar and ZXing) were not executed on raw, unlocalized full images. Instead, they were evaluated strictly on the exact same localized ROIs extracted by the YOLOv11s detector.

Pyzbar achieved a read rate of 36.41%, successfully decoding 4388 of the 12,050 barcodes, all of which exactly matched the corresponding ground-truth values. ZXing performed substantially better, decoding 9361 barcodes with a read rate of 77.68%, all of which also exactly matched the corresponding ground-truth values. However, both libraries exhibited reduced performance under severe barcode degradation. The proposed framework successfully decoded 11,585 barcodes, corresponding to a read rate of 96.14%. Of these, 11,569 barcodes exactly matched the ground-truth values, resulting in an exact

decoding accuracy of 96.01%. In terms of read rate, this corresponds to improvements of 18.46 and 59.73 percentage points over ZXing and Pyzbar, respectively.

TABLE II: COMPARISON OF DECODING PERFORMANCE

Method	Decoded	Exact Decoded	Read Rate (%)	Exact Accuracy (%)	Time/Barcode
Pyzbar	4388	4388	36.41	36.41	0.0075
ZXing	9361	9361	77.68	77.68	0.0010
Proposed method	11,585	11,569	96.14	96.01	0.3817

The performance gain can be attributed to the combination of the multi-stage decoding architecture and the proposed signal-based reconstruction method. By exploiting barcode periodicity in the signal domain, the framework is able to recover barcode information that remains inaccessible to conventional image-based decoding approaches. The framework produced 11,585 valid 10-digit outputs, of which 11,569 exactly matched the corresponding ground-truth values. All decoded outputs were compared against the corresponding ground-truth values derived from the Human-Readable Interpretation (HRI) printed on each baggage tag. This characteristic is particularly important in safety-critical applications such as airport baggage reconciliation.

Although the proposed framework requires additional computational cost, the substantial improvement in decoding reliability justifies the overhead in applications where accuracy and robustness are prioritized.

C. Decoding Pipeline Analysis

A stage-wise analysis was conducted on the complete dataset of 12,050 barcodes to quantify the contribution of each component in the proposed decoding pipeline. The contribution of each decoding stage is quantified below.

Direct library decoding successfully recognized 4373 barcodes with negligible computational overhead, demonstrating the effectiveness of the early-exit strategy for high-quality samples. Image enhancement provided the largest improvement, recovering 6612 additional barcodes and increasing cumulative read rate from 36.29% to 91.16%. This result suggests that many decoding failures were primarily caused by reduced contrast and uneven illumination rather than irreversible structural damage.

Multi-library decoding recovered a further 420 barcodes, increasing cumulative read rate to 94.65%. The improvement highlights the complementary strengths of different preprocessing configurations and decoding libraries under diverse degradation conditions.

Signal-based reconstruction recovered an additional 180 severely degraded barcodes, increasing overall read rate to 96.14%. Since this stage is activated only for barcode instances that remain unresolved after the preceding stages, the proposed early-exit architecture effectively limits the use of computationally intensive recovery procedures.

To comprehensively assess the computational cost of the proposed framework, a detailed timing analysis was conducted. The YOLOv11s detector requires an average inference time of 39.1 ms per image, while the subsequent barcode decoding pipeline requires an average of 0.3817 s per barcode. The processing-time distribution and step-wise computational contributions of the decoding pipeline are shown in Fig. 5. In addition, Table III summarizes the number of barcodes successfully decoded and the cumulative processing time associated with each decoding stage.

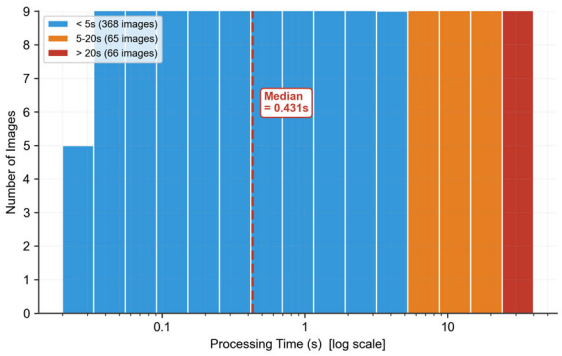

(a)

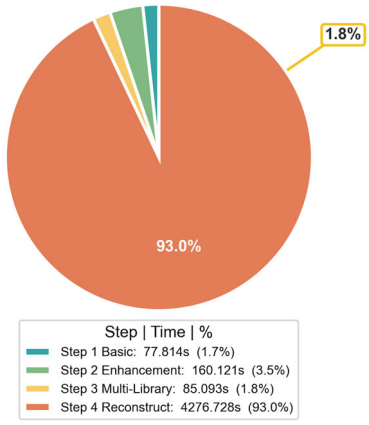

(b)

Fig. 5. Processing time analysis: (a) processing time distribution and (b) time breakdown for each step.

TABLE III: STEP-BY-STEP IMPROVEMENT (OVERALL ABLATION STUDY)

Step	Solved	Cumulative Solved	Read Rate (%)	Total Time (s)
step1_basic	4373	4373	36.29	77.814
step2_enhancement	6612	10,985	91.16	160.121
step3_multi_library	420	11,405	94.65	85.093
step4_reconstruct	180	11,585	96.14	4276.728

Overall, the results demonstrate that the proposed framework effectively combines lightweight decoding, image enhancement, multi-library processing, and signal-domain reconstruction within a unified early-exit architecture. The proposed framework successfully produced readable 10-digit outputs for 11,585 out of 12,050 barcode instances, corresponding to a read rate of

96.14%. After comparison with the ground-truth barcode values, 16 of these decoded outputs were found to contain one or more incorrect characters due to extreme degradation. Therefore, 11,569 instances exactly matched the ground truth, resulting in an exact decoding accuracy of 96.01%, which is consistently reported as the primary overall performance metric throughout the manuscript. The corresponding stage-wise decoding performance is shown in Fig. 6.

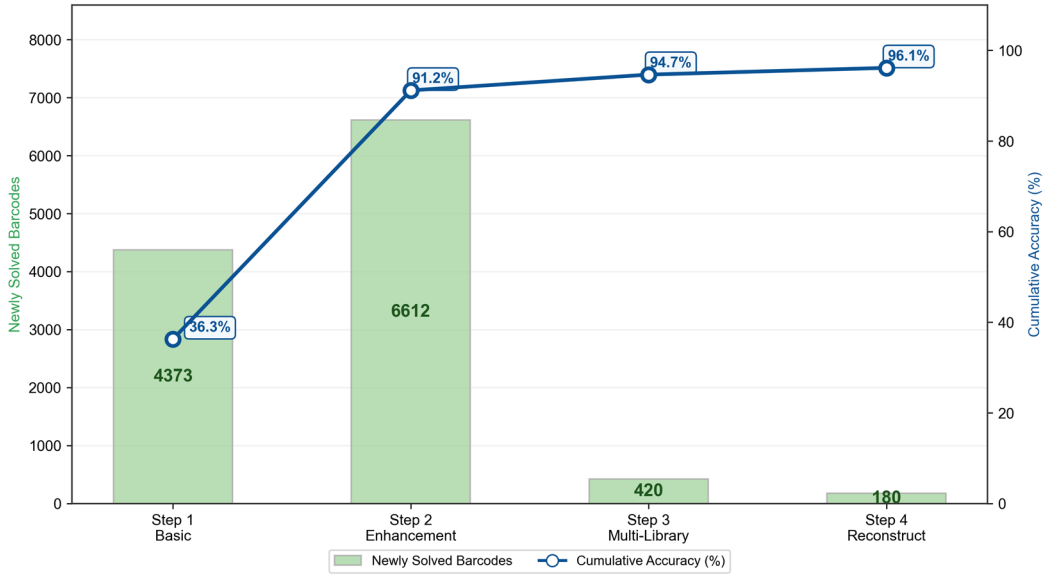

Fig. 6. Stage-wise decoding performance of the proposed framework on 12,050 ITF barcodes.



Fig. 7. Examples of successfully decoded and failed barcode instances from the airline baggage dataset.

D. Statistical Validation

To further validate the reliability of the proposed framework, statistical analysis was performed on the decoding results of all 12,050 barcode instances. The proposed method achieved an overall decoding accuracy of 96.01%, with a 95% Confidence Interval (CI) of [95.66%, 96.36%]. Furthermore, McNemar's test was conducted to evaluate the statistical significance of the performance difference between the proposed framework and the strongest baseline library, ZXing. The test yielded a chi-square statistic of $\chi^2 = 2194.08$ with $p < 0.0001$, indicating that the observed difference in decoding performance between the two methods is statistically significant.

E. Failure Analysis of Unsuccessful Barcode Decoding

Despite achieving an exact decoding accuracy of 96.01%, 481 barcode instances did not exactly match the ground truth. Analysis of these failures revealed three primary causes: severe structural damage, incomplete barcode visibility, and extreme fading, as illustrated in

Fig. 7. The figure shows representative examples from the airline baggage dataset, where green boxes indicate successfully decoded barcodes and red boxes denote decoding failures.

The most significant failures occurred when large portions of the barcode were physically missing or obscured by strong reflections, preventing reliable preservation of the module-width relationships required for ITF decoding. Several examples in Fig. 7 exhibit severe physical damage, contamination, and reflection artifacts that disrupt barcode continuity. A second failure mode involved partially visible barcodes near image boundaries, where cropping removed critical elements such as quiet zones or start/stop patterns. The remaining failures were associated with extremely faded, low-contrast barcodes, for which the intensity difference between bars and background approached the noise level, limiting reliable segmentation even after enhancement and reconstruction. Although the proposed framework successfully recovered many degraded barcode instances, insufficient structural information remained available in these cases for reliable signal reconstruction and subsequent decoding.

To provide deeper quantitative insight into the limitations of the proposed framework, measurable image degradation metrics were extracted from all 12,050 barcode crops. Among these samples, 11,569 were decoded exactly, while 481 did not exactly match the ground truth. The successfully decoded barcodes exhibited higher average Laplacian variance (393.73), RMS contrast (36.44), and Otsu foreground-background contrast (87.75). In contrast, the failed instances exhibited lower average values of 241.39, 29.35, and 67.94, respectively. These results indicate that the remaining decoding failures are associated with more severe blur and contrast degradation, providing a quantitative characterization of the conditions under which the proposed VPP-based reconstruction approach becomes less effective.

Table IV compares the proposed framework with representative recent barcode analysis methods reported in the literature. Recent studies have explored barcode localization using lightweight YOLO-based detectors [14, 17], image restoration through deep-learning-based deblurring techniques [18], and end-to-end frameworks that integrate barcode localization and decoding using deep learning approaches [20]. These methods have demonstrated promising performance under specific operating conditions, including mobile-device deployment, image restoration, and UAV-based barcode recognition. However, most existing approaches primarily focus on individual components of the barcode processing workflow, such as detection, restoration, or end-to-end decoding, without explicitly exploiting barcode structural information in the signal domain.

In contrast, the proposed framework combines deep-learning-based localization with a progressive four-stage decoding pipeline and a novel signal-based reconstruction module. Rather than relying solely on image-domain enhancement, the proposed method exploits barcode periodicity in the one-dimensional signal domain to recover structural information from severely degraded barcode regions. This design enables robust decoding under challenging real-world conditions while maintaining compatibility with conventional barcode readers.

Although direct numerical benchmarking on the exact same dataset is currently not feasible because the corresponding source codes are not publicly available in several cases or the reported evaluations use private datasets and different barcode symbologies, Table IV summarizes the quantitative performance metrics reported in the corresponding studies. These results provide an indirect quantitative comparison while accounting for differences in datasets, barcode types, and experimental protocols. The statistical validation of the proposed framework further provides quantitative evidence of its performance relative to the baseline decoder.

TABLE IV: COMPARISON WITH PREVIOUS WORK

Study	Task	Method	Reported Performance
Li *et al*. [14]	Detection	YOLO-based localization	mAP@0.5 of 97.8%, Precision of 96.4%, and Recall of 93.9%
Ershova *et al*. [17]	Detection	YOLO-Barcode	F1-score of 98.6% on the ZVZ-real dataset and 4× faster inference
Shi *et al*. [18]	Restoration + Decoding	DeblurGAN-v2 barcode deblurring	Improved decoding rate by 27.2% (Zbar) and 10.4%
Alsulami & Jhanjhi [20]	Localization + Decoding	Deep-learning framework	mAP of 92.4% under simulated UAV conditions
This work	Detection + Decoding	YOLOv11s + 4-stage pipeline + signal-based reconstruction	99.61% precision for localization and 96.01% exact decoding accuracy

IV. CONCLUSION

This study presented an automated barcode decoding framework that combines YOLOv11s-based localization with a four-stage decoding pipeline for robust recognition of degraded barcode images and is specifically tailored for Interleaved Two of Five (ITF) barcodes. The YOLOv11s detector demonstrated excellent localization performance, achieving 99.61% precision and 99.3% mAP@0.5, thereby providing reliable barcode region extraction under challenging imaging conditions.

Evaluated on 12,050 real-world ITF barcodes collected from an airline baggage-handling environment, the proposed framework achieved an exact decoding accuracy of 96.01%, substantially outperforming ZXing and Pyzbar. The results demonstrate that the progressive decoding architecture effectively balances accuracy and efficiency through an early-exit strategy, while the proposed signal-based reconstruction method successfully recovers

severely degraded barcodes that remain unreadable using conventional image-based techniques.

The proposed framework was evaluated exclusively on ITF barcodes because this symbology is used in the airline baggage-handling environment targeted by this research. Although the proposed signal-based reconstruction strategy was designed for degraded one-dimensional barcode signals, its performance on high-density symbologies such as Code 128 and EAN-13 has not yet been experimentally validated. The narrower bars and smaller module widths of these symbologies may introduce increased horizontal signal bleeding and require adaptive signal-processing parameters. Therefore, the reported experimental results and performance claims in this study are specific to the evaluated ITF barcode symbology and the real-world conditions considered. Future work will therefore investigate the applicability of the proposed VPP framework to a broader range of barcode symbologies, together with adaptive parameter optimization and GPU acceleration for improved computational efficiency.

Conflict of Interest

The authors declare no conflict of interest.

Author Contributions

Panupong Chaiyarat conducted the experimental measurements and data collection; Chaiyong Soemphol designed the research methodology and supervised the study; all authors analyzed the data, wrote the manuscript, and approved the final version.

Acknowledgment

This research was supported by the Mahasarakham University, Thailand.

References

[1] J. Kubáňová, I. Kubasáková, K. Čulík, and L. Štítik, "Implementation of barcode technology to logistics processes of a company," *Sustainability*, vol. 14, no. 2, 790, 2022.

[2] D. J. Closs and K. Xu, "Logistics information technology practice in manufacturing and merchandising firms: An international benchmarking study versus world class logistics firms," *Int. J. Phys. Distrib. Logist. Manag.*, vol. 30, no. 10, pp. 869–886, 2000.

[3] Z. Hasibuan, A. S. Putra, M. T. Multazam, and A. F. Yulianto, "The implementation of barcode on warehouse management system for warehouse efficiency," *J. Phys. Conf. Ser*., vol. 1573, no. 1, 012038, 2020.

[4] Y. Liu, W. Li, and X. Gao, "Barcode type classification using convolutional neural networks," *IEEE Access*, vol. 8, pp. 69890–69900, 2020.

[5] R. Shams and P. Sadeghi, "Bar code recognition in highly distorted and low resolution images," in *Proc. IEEE Int. Conf. Acoust., Speech Signal Process. (ICASSP)*, 2007, pp. I-737–I-740.

[6] I. M. Mohammed and N. A. M. Isa, "Contrast limited adaptive local histogram equalization method for poor contrast image enhancement," *IEEE Access*, vol. 13, pp. 62600–62632, 2025.

[7] M. Katona, "A survey of barcode recognition and detection methods," *Sensors*, vol. 17, no. 2, 247, 2017.

[8] J. Zhu, Y. Ye, C. Lai, and J. Jiang, "Real-time barcode detection for embedded IoT systems using lightweight YOLO architecture," *J. Real-Time Image Process*., vol. 23, 78, 2026.

[9] X. Tang, K. Tang, K. Sun, W. Gu, and L. Xiang, "EBP-YOLOv5: Channel pruning-based lightweight YOLOv5 for QR code detection," *Signal Image Video Process.*, vol. 18, no. 12, pp. 9515–9526, 2024.

[10] A. Namane and A. Al-Dahoud, "Comparative study of YOLO versions for barcode detection on product images," *Int. J. Adv. Comput. Sci. Appl.,* vol. 12, no. 5, pp. 540–547, 2021.

[11] D. K. Hansen, K. Nasrollahi, C. B. Rasmussen, and T. B. Moeslund, "Real-time barcode detection and classification using deep learning," in *Proc. 9th Int. Joint Conf. Comput. Vis., Imag. Comput. Graph. Theory Appl. (IJCCI)*, 2017, pp. 321–327.

[12] Y. Xiao and Z. Ming, "1D barcode detection via integrated deep-learning and geometric approach," *Appl. Sci.*, vol. 9, no. 16, 3268, 2019.

[13] T.-Y. Lin, P. Dollár, R. Girshick, K. He, B. Hariharan, and S. Belongie, "Feature pyramid networks for object detection," in *Proc. IEEE Conf. Comput. Vis. Pattern Recognit. (CVPR)*, Honolulu, HI, USA, 2017, pp. 936–944.

[14] C. Li, Q. Zeng, and L. Lu, "Lightweight barcode positioning algorithm based on YOLO model," *IEEE Access*, vol. 12, pp. 192341–192355, 2024.

[15] Y. Qu and F. Zhang, "MGL-YOLO: A lightweight barcode target detection algorithm," *Sensors*, vol. 24, no. 23, 7590, 2024.

[16] R. Wudhikarn, P. Charoenkwan, and K. Malang, "Deep learning in barcode recognition: A systematic literature review," *IEEE Access,* vol. 10, pp. 8049–8072, 2022.

[17] D. M. Ershova, A. V. Gayer, P. V. Bezmaternykh, and V. V. Arlazarov, "YOLO-Barcode: Towards universal real-time barcode detection on mobile devices," *Comput. Opt.,* vol. 48, no. 4, pp. 592–600, 2024.

[18] C. Shi, Y. Wang, Z. Zhang, and X. Li, "Real-time multi-scale barcode image deblurring based on improved DeblurGAN-v2," *Electronics*, vol. 14, no. 7, 1298, 2025.

[19] J. Chen, H. Li, Y. Wang, and X. Zhao, "A lightweight barcode detection algorithm based on deep learning," *Appl. Sci.,* vol. 14, no. 22, 10417, 2024.

[20] F. Alsulami and N. Z. Jhanjhi, "Deep learning framework for barcode localization and decoding using simulated UAV imagery," *Sci. Rep.,* vol. 16, 399, 2025.

[21] K. K. Pappula and S. Anasuri, "Deep learning for industrial barcode recognition at high throughput," *Int. J. AI Data Sci. Mach. Learn*., vol. 5, no. 1, 2024.

[22] G. Bradski and A. Kaehler, *Learning OpenCV 3*, Sebastopol, CA, USA: O'Reilly Media, 2016.

[23] Y. Zhou and B. Zhao, "You Only Look Once 11 (YOLO11) optimizations for lightweight and accurate plant detection in uncrewed aerial vehicle imagery," *PeerJ Comput. Sci.*, vol. 11, e3322, 2025.

[24] S. J. Reddi, S. Kale, and S. Kumar, "On the convergence of Adam and beyond," in *Proc. Int. Conf. Learn. Represent. (ICLR)*, 2018.

[25] S. M. Pizer et al., "Adaptive histogram equalization and its variations," *Comput. Vision Graph. Image Process*., vol. 39, no. 3, pp. 355–368, Sep. 1987.

[26] R. C. Gonzalez and R. E. Woods, *Digital Image Processing*, 4th ed. Hoboken, NJ, USA: Pearson, 2018.

[27] N. Otsu, "A threshold selection method from gray-level histograms," *IEEE Trans. Syst., Man, Cybern.*, vol. 9, no. 1, pp. 62–66, Jan. 1979.

Copyright © 2026 by the authors. This is an open access article distributed under the Creative Commons Attribution License which permits unrestricted use, distribution, and reproduction in any medium, provided the original work is properly cited (CC BY 4.0).



Panupong Chaiyarat received the B.Sc. in computer science (2019) from Mahasarakham University, Thailand. He is currently pursuing the M.Eng. in electrical and computer engineering at Mahasarakham University, Thailand. His research interests include computer vision, deep learning, digital image processing, and automated barcode recognition. He is currently a frontend developer at Terminal 8.



Chaiyong Soemphol received the B.Eng. in electrical engineering from Khon Kaen University, Thailand in 2011. He also received his Ph.D. in electrical engineering from Khon Kaen University, Thailand in 2017. Since 2018, he has been with the Department of Electrical Engineering, Faculty of Engineering, Mahasarakham University, Maha Sarakham, Thailand as a Lecturer. His research interests include compact microstrip devices, metamaterial applications for RF, RF measurement techniques, microwave sensor, wireless power transfer systems, renewable energy, and electromechanical energy conversion.